


Article

Non-Invasive Rapid Detection of Lung Cancer Biomarker Toluene with a Cataluminescence Sensor Based on the Two-Dimensional Nanocomposite Pt/Ti₃C₂T_x-CNT

Hongyan Wang ^{1,*}, Xiaoqi Shi ¹, Fei Liu ², Tingmei Duan ¹ and Bai Sun ^{2,3,*} 

¹ Department of Radiation Oncology, The First Affiliated Hospital of Anhui Medical University, Hefei 230022, China

² Engineering Research Center of Building Energy Efficiency Control and Evaluation of the Ministry of Education, College of Environment and Energy Engineering, Anhui Jianzhu University, Hefei 230601, China

³ Nano-Materials and Environmental Detection Laboratory, Hefei Institute of Physical Science, Chinese Academy of Sciences, Hefei 230031, China

* Correspondence: whhy5000@163.com (H.W.); bsun@iim.ac.cn (B.S.); Tel.: +86-551-63828252 (B.S.)

Abstract: A novel two-dimensional nanocomposite Pt/Ti₃C₂T_x-CNT was synthesized for the non-invasive rapid detection of toluene, a lung cancer biomarker, via cataluminescence (CTL). Pt/Ti₃C₂T_x-CNT exhibited a good catalytic performance toward toluene. The CTL sensor based on Pt/Ti₃C₂T_x-CNT has the advantage of rapid response: The average response time was about 1 s, and the average recovery time was about 30 s. Moreover, the material has a wide scope of detection for toluene, and the limit of detection defined as 3 S/N was about 2 ppm. The optimal working temperature (150 °C) is lower than common sensors, so it has a broad prospect in the actual detection process. Aside from its weak response to formaldehyde, the sensor only exerted a strong response signal to toluene, and no response was observed to other VOCs, indicating that this CTL sensor has good selectivity for toluene. The possible sensing mechanism of CTL showed that toluene was oxidized to generate excited-state CO₂^{*}, which emitted a luminescent signal when it returned to the ground state.

Keywords: MXene; nanocomposites; cataluminescence; detection of toluene



Citation: Wang, H.; Shi, X.; Liu, F.; Duan, T.; Sun, B. Non-Invasive Rapid Detection of Lung Cancer Biomarker Toluene with a Cataluminescence Sensor Based on the Two-Dimensional Nanocomposite Pt/Ti₃C₂T_x-CNT. *Chemosensors* **2022**, *10*, 333. <https://doi.org/10.3390/chemosensors10080333>

Academic Editor: Tae Geun Kim

Received: 11 July 2022

Accepted: 8 August 2022

Published: 14 August 2022

Publisher's Note: MDPI stays neutral with regard to jurisdictional claims in published maps and institutional affiliations.



Copyright: © 2022 by the authors. Licensee MDPI, Basel, Switzerland. This article is an open access article distributed under the terms and conditions of the Creative Commons Attribution (CC BY) license (<https://creativecommons.org/licenses/by/4.0/>).

1. Introduction

Human respiration contains a large number of gases, including carbon dioxide (CO₂), ammonia (NH₃), ethanol (C₂H₅OH), acetone (CH₃COCH₃), and toluene (C₇H₈) [1]. The human-exhaled breath serves to exhaust the body of its metabolic byproducts. These byproducts may be unique in lung cancer, based on metabolic changes within or around cancer cells or due to metabolic changes in the immunological system of the body [2]. Careful analysis of such breathing gases by using reliable detection equipment (such as gas sensors) provides a non-invasive way to check people's health: a significantly high level of gas can be used as a biomarker for pathogenic development (e.g., toluene: lung cancer; acetone: diabetes; ammonia: kidney problems) [3–5]. The development of toluene gas sensors for biomarker applications has attracted particular attention because this medical device can provide a non-invasive tool for the daily monitoring of lung cancer patients [6,7].

At present, there are many methods and technologies that can be used to detect toluene gas. However, when other respiratory gases coexist, the sensitivity and selectivity for the detection of low concentration toluene is still a challenging topic. The existing methods of toluene detection have some drawbacks and cannot achieve rapid detection [8–12]. For example, the chemical detection method takes a long time, and the interference of homologues cannot be ruled out. The infrared spectroscopy method has low sensitivity and large relative error and needs a large number of representative samples to model before detection [9]. Gas chromatography is expensive and requires professional operation [10].

Therefore, it is necessary to establish a rapid, portable, and sensitive detection method for toluene [8]. CTL refers to the phenomenon according to which when a catalytic oxidation reaction occurs at the gas–solid interface, the substance absorbs energy from the ground state and converts it into an excited state, and the excited state releases energy into the ground state, accompanied by chemiluminescence [13]. The CTL method based on nanomaterials is a new sensor detection method, which is widely studied and applied to the detection of volatile organic compounds (VOCs) in the environment [14–19]. Shi et al. [20] prepared Pt/NU-901 nanocomposites for CTL sensors to detect acetone, a marker of diabetes. The detection method is stable, fast, and accurate. Yu et al. [21] reported a camellia-like NiO and used it in a CTL sensor for the rapid detection of H₂S. The large specific surface area of the material, its developed porous structure, and the effect of surface-adsorbed oxygen make the sensor have high sensitivity and selectivity for H₂S detection. This method has high sensitivity, selectivity, and fast detection speed. There is no need to add other reagents when using a CTL sensor to detect VOCs. In addition, sensing elements are not consumed in the CTL reaction process, so the nanomaterial can be reused as a sensing element, which enables the CTL sensor to monitor VOCs in real time [13,22–25]. Therefore, CTL-based sensors can be applied to the detection of toluene.

MXene is a novel two-dimensional material for transition metal carbides or nitrides obtained by using fluoride etching MAX (where M is an early transition metal carbide, A represents the main group elements, and X represents C and/or N elements [26]) ternary layered materials, which has attracted increasing attention because of its unique structure and excellent electrical and optical properties [27]. A single, large layer and less defective Ti₃C₂T_x sheet can be separated via simple ultrasonication or manual shaking by etching with hydrochloric acid and lithium fluoride [28–30]. Additionally, carbon nanotubes (CNTs) have excellent sensing properties [31,32], and metal decoration can improve sensing performance. In recent years, the preparation and exploration of MXene-based composites have started to become research hotspots [33]. In addition, Pt and other precious metals have been widely studied because of their unique physical and chemical properties. Research shows that Pt has good oxidation resistance and high conductivity, and platinum can provide excitation electrons in CTL sensors. Therefore, adding it to a CTL sensor will further enhance the detection signal of the sensor and speed up its response and recovery time [19,34–36]. Therefore, Pt was used as decoration to prepare Pt/Ti₃C₂T_x-CNT catalyst in this paper. Then, the CTL characteristics of toluene on the surface of Pt/Ti₃C₂T_x-CNT were determined, and the optimal detection conditions of toluene were investigated using an ultraweak chemiluminescence analyzer.

2. Experiment

2.1. Reagents and Instruments

The reagents used in this experiment were lithium fluoride (LiF), cetyltrimethylammonium bromide (CTAB), ethanol, chloroplatinic acid (H₂PtCl₆·6H₂O), sodium borohydride (NaBH₄), toluene, formaldehyde, chloroform, cyclohexane, tetrachloroethane, diethyl ether, acetone, and ammonia, which were purchased from Sinopharm Chemical Reagent Co., Ltd., (Shanghai, China) and used as received, without further purification. Ti₃AlC₂ was from Kayene Ceramics Co., Ltd., (Yantai, China). CNT was purchased from Beijing Boyu Co., Ltd., (Beijing, China). Deionized water was prepared using FST-TOP-A24 super-pure water equipment made by Shanghai Fushite Instrument Equipment Co., Ltd., (Shanghai, China).

The instruments used in the experiment included an RCT basic magnetic stirrer (EKA Instrument Equipment Co., Ltd., Guangzhou, China), a TG16K-II table high-speed centrifuge (Shanghai Zhaodi Biotechnology Co., Ltd., Shanghai, China), a DHG-9023A air-drying box (Shanghai YiHeng Scientific Instrument Co., Ltd., Shanghai, China), and a PHB-3 digital pH meter (Shanghai SanXin Instrument Factory, Shanghai, China).

2.2. Preparation of Pt/Ti₃C₂T_x-CNT Catalysts

The etching methods of Pt/Ti₃C₂T_x-CNT have been reported in previous studies [37–39].

2.2.1. Preparation of $Ti_3C_2T_x$

First, 0.8 g of LiF was added to a 10 mL HCl (9 mol/L) solution; then, 0.5 g of Ti_3AlC_2 was added and mixed into the solution with continuous stirring at 35 °C for 24 h. The reaction precipitate was repeatedly washed with deionized (DI) water until the pH value of the supernatant was greater than 6. Finally, the precipitate was dissolved in the DI water, and the resulting solution was sonicated in an Ar atmosphere for 1 h.

2.2.2. Preparation of CTAB-CNT

Briefly, 50 mg CNT was added to 100 mg CTAB, and then the mixture was ultrasonically dispersed in 50 mL DI water. After the reaction was complete, the precipitate was washed with ethanol several times to remove the residual CTAB. Finally, centrifugation (9000 rpm, 15 min) was used to collect the black precipitate; thus, the CTAB-CNT was obtained.

2.2.3. Preparation of Pt/ $Ti_3C_2T_x$ -CNT

First, 40 mg $Ti_3C_2T_x$ and 40 mg CTAB-CNT were dispersed in 40 mL DI water to obtain the $Ti_3C_2T_x$ -CNT. Then, $H_2PtCl_6 \cdot 6H_2O$ was added dropwise to the $Ti_3C_2T_x$ -CNT suspension and stirred continuously for 2 h at room temperature. Finally, an excess of $NaBH_4$ solution was added to the above solution to react until no bubbles were produced. After centrifugation, washing, and drying, the Pt/ $Ti_3C_2T_x$ -CNT catalyst was obtained.

2.3. Characterization

The morphology and structure of Pt/ $Ti_3C_2T_x$ -CNT were investigated using a scanning electron microscope (SEM, Zeiss Auriga FIB-SEM, 10 kV) and a transmission electron microscope (TEM, JEOL-2010, 200 kV). The chemical composition was determined with an energy-dispersive spectrometer (EDS). X-ray diffraction (XRD) patterns were recorded using a Philips X'Pert PRO MPD diffractometer with a Cu K α X-ray source ($\lambda = 1.5405 \text{ \AA}$).

2.4. Cataluminescence Sensing Measurement

Pt/ $Ti_3C_2T_x$ -CNT was coated on ceramic rods and then placed in a reaction chamber. An adjustable transformer was used to heat the reaction chamber, and a flow pump was used to adjust the airflow rate. In the same reaction condition, using a syringe, 10 kinds of VOCs (toluene, trichloromethane, tetrachloroethane, cyclohexane, formaldehyde, diethyl ether, acetone, carbon dioxide, ammonia, and ethanol) were injected into the reaction chamber to react with Pt/ $Ti_3C_2T_x$ -CNT, and the CTL value in Pt/ $Ti_3C_2T_x$ -CNT surface was determined using an ultraweak chemiluminescence analyzer (BPCL-1-TIC, Guangzhou Microphotonics Technologies Co., Ltd., Guangzhou, China). The sensing device is shown in Figure 1.

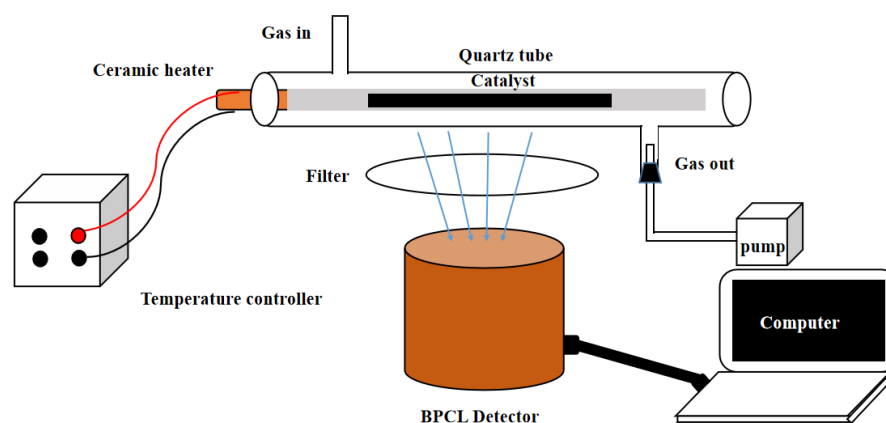


Figure 1. Schematic diagram of CTL sensor experimental device.

The dry air required for the experiment was provided by a compressed gas cylinder and carried out under the condition of constant humidity ($40 \pm 5\%$). The temperature was adjusted and detected using the adjustable transformer. The ceramic heating rods coated with nanomaterials were put in a closed quartz tube (500 mL), and the airflow rate was adjusted by adjusting the cylinder valve. The gas flow rate was detected with a rotor gas flowmeter (anti-corrosion LZB-3WBF). Finally, the gas solution to be tested was injected into the cylinder through a micro syringe and then delivered to the reaction chamber. The generated catalytic luminescence signal was detected and processed via a photoelectric detection and data processing system. The measurement wavelength of this experiment was the effective response wavelength (300–650 nm) that can be detected by the photomultiplier tube in the BPCL ultraweak microluminescence instrument, so no specific wavelength was selected. The concentration of the detected gas in the experiment is calculated by the following formula [40]:

$$C = \frac{V_i \times P_0}{V_c \times P_a} \quad (1)$$

where C is the concentration of the gas to be measured, V_i is the volume of the gas to be measured sucked into the syringe, V_c is the volume of the reaction chamber, P_0 is the vapor pressure of the gas to be measured at room temperature, and P_a is the standard atmospheric pressure.

3. Results and Discussions

3.1. Characterization of Pt/Ti₃C₂T_x-CNT

Figure 2a–e show the SEM images of Pt/Ti₃C₂T_x-CNT and its corresponding EDS mapping. As can be seen from Figure 2a–e, the material consists of Ti, Pt, O, and C. In this composition, Ti and O are Ti₃C₂T_x feature elements, C is a Ti₃C₂T_x and CNT feature element, and Pt is the material surface decoration element. The content of each element is shown in Table 1. Figure 2f,g correspond to the SEM and TEM images of the material. As can be seen from Figure 2f,g, the material has a tubular structure connected by nodes, which shows that the CNT and Ti₃C₂T_x are closely combined to form a stable structure. There is Ti with partial solubility on the surface of Ti₃C₂T_x, which makes the Ti cation separate from the Ti₃C₂T_x substrate and freely dissolve into the solution, so Ti₃C₂T_x has a negative charge [26], while the CNT modified with cationic surfactant CTAB has a positive charge [41]. The positively charged CNT and negatively charged Ti₃C₂T_x are combined via electrostatic interaction. Research has shown that the composite of Ti₃C₂T_x and CNT can increase the active sites of the material and improve the cycle life of the material [26,41]. In addition, Pt was attached to the surface of the nanotubes, which indicates that the Pt/Ti₃C₂T_x-CNT catalyst was successfully prepared in this experiment.

Table 1. Content of elements in Pt/Ti₃C₂T_x-CNT.

Elements	Weight%	Atomic%
C	9.76	93.83
O	0.75	5.39
Ti	0.18	0.44
Pt	0.59	0.34
Totals	11.28	1

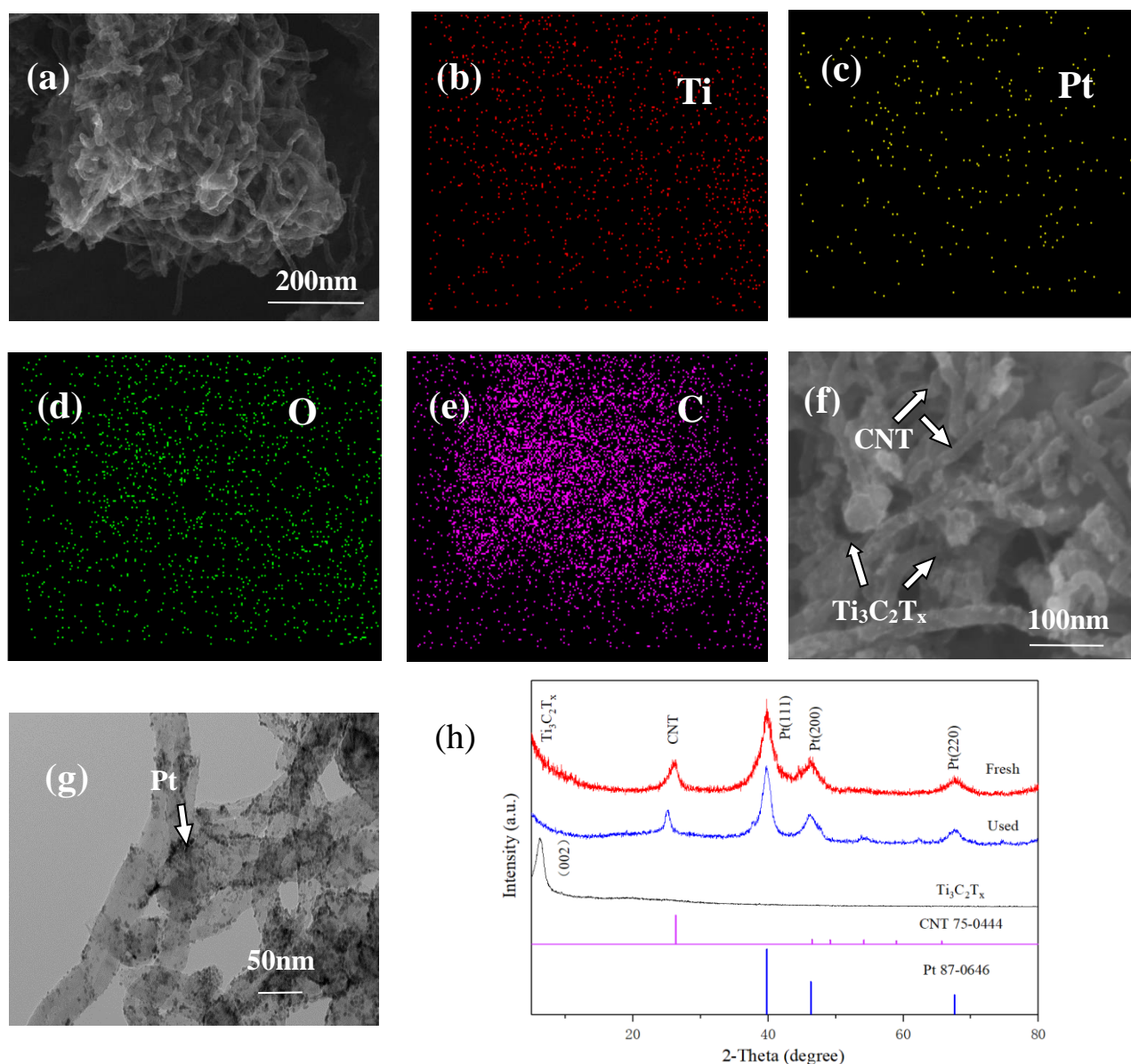


Figure 2. (a–e) SEM images and EDS mapping of Pt/Ti₃C₂T_x-CNT; (f,g) SEM and TEM images of Pt/Ti₃C₂T_x-CNT; (h) XRD pattern of Pt/Ti₃C₂T_x-CNT.

The XRD pattern of Pt/Ti₃C₂T_x-CNT is shown in Figure 2h. As can be seen from Figure 2h, the diffraction peaks of the materials appeared at 6.3°, 26.3°, 39.8°, 46.3°, and 67.5°, respectively. Diffraction peaks matched well the corresponding standard cards. Among them, the diffraction peak of 6.2° corresponded to Ti₃C₂T_x, and 26.3° corresponded to the characteristic peak of CNT (JCPDS No.75-04444). In addition, the diffraction peaks of 39.8°, 46.3°, and 67.8° corresponded to the basal planes of Pt (111), Pt (200), and Pt (220) (JCPDS No.87-0646). No other impurities were observed in the XRD pattern.

3.2. CTL Response of Toluene on Pt/Ti₃C₂T_x-CNT

Figure 3a shows the luminescence intensity upon exposure to toluene vapors of the Pt/Ti₃C₂T_x-CNT material. After the sensor was debugged and stabilized, the CTL strength was measured. The CTL strength produced by toluene before adding toluene was 0, and after adding toluene, the CTL strength produced by toluene on the material surface could reach about 175,000, with an average response time of 1 s and average recovery time of 30 s. When the CTL strength was restored to 0, toluene was added again, and the CTL strength

immediately produced was basically unchanged, indicating that Pt/Ti₃C₂T_x-CNT has a good CTL response to toluene. In addition, under the same experimental conditions, after four times of repeated tests, no significant change was observed in signal strength, which shows that the CTL sensor has good reproducibility and high stability. Figure 3b shows the luminous intensity of Ti₃C₂T_x-CNT when exposed to toluene vapor. From the comparison of Figure 3a,b, it can be seen that the luminous intensity of Ti₃C₂T_x-CNT exposed to toluene vapor was significantly lower than that of Pt/Ti₃C₂T_x-CNT exposed to toluene vapor, indicating that the addition of Pt was conducive to the CTL signal detection of toluene and accelerated the corresponding recovery time. The CTL-based method has obvious advantages for the detection of VOCs, such as sensitive and rapid detection. However, research on the detection of toluene via CTL is relatively scarce [19,42,43], so the material has great potential application value.

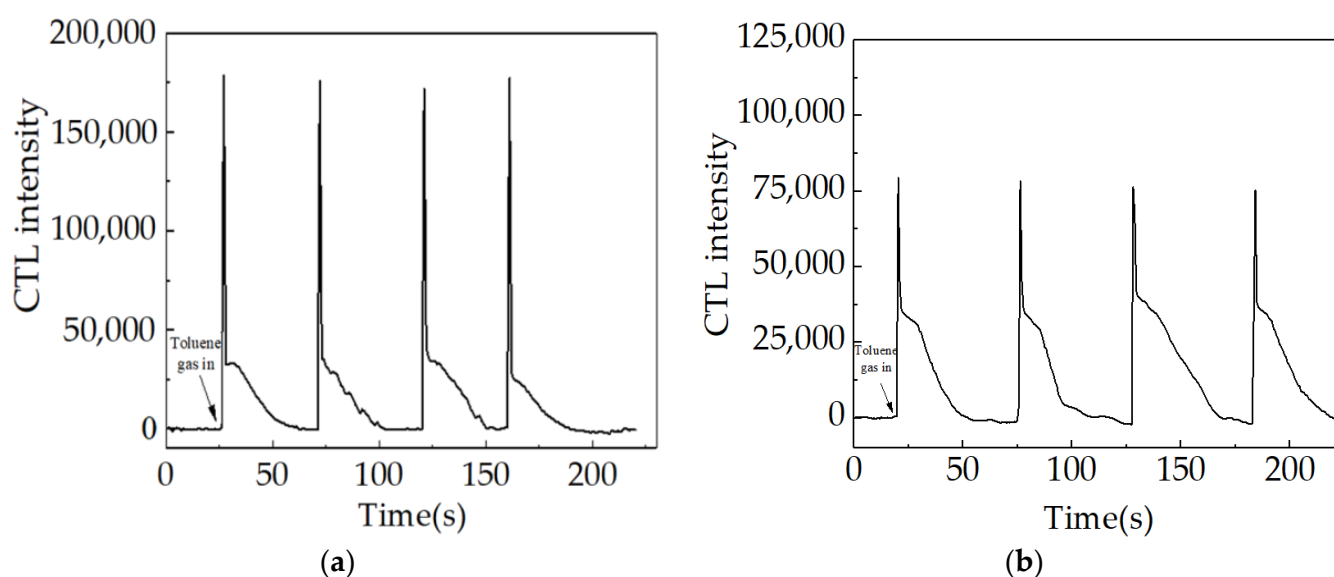


Figure 3. (a) The luminescence intensity upon exposure to toluene vapors of Pt/Ti₃C₂T_x-CNT material; (b) the luminescence intensity upon exposure to toluene vapors of Ti₃C₂T_x-CNT material. (detecting concentration: 87 ppm. Working temperature: 150 °C. Airflow rate: 200 mL/min).

3.3. Optimization of CTL Sensor

Temperature is an important factor for CTL reactions, and the CTL value generally increases with the temperature. However, with the increase in temperature, the noise of the detection device also increases. In addition, the high temperature may affect the structure of the material [44]. Therefore, it is necessary to study the optimal working temperature.

The effects of operating temperature on CTL intensity and the S/N [45] value are shown in Figure 4a. The CTL intensity of toluene on the Pt/Ti₃C₂T_x-CNT surface increased with the increase in temperature under certain concentrations and airflow rates. At the same time, the S/N value first increased with the increase in temperature and then decreased after 150 °C, which implies that 150 °C is the optimal temperature for the detection of toluene. Therefore, the temperature of 150 °C, which occurs at a large luminescent signal area for toluene, was chosen in subsequent experiments.

The airflow rate has also an obvious influence on CTL strength. A slow air flow rate leads to a low effective contact concentration between the detector and the material, and a high airflow rate causes the detector to be taken out of the reaction chamber before it can react with the material.

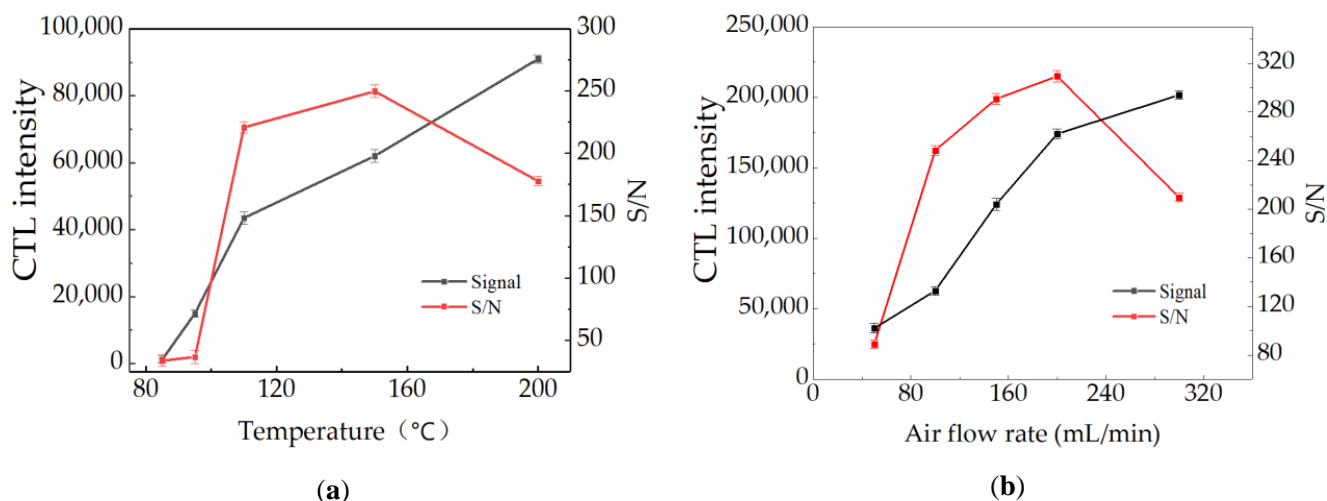


Figure 4. Effects of (a) working temperature and (b) airflow rate on CTL intensity and the S/N value: (a) detecting concentration: 87 ppm; airflow rate: 100 mL/min; (b) detecting concentration: 87 ppm; detecting temperature: 150 °C.

At different gas flow rates, the CTL strength between toluene and the material was detected via BPCL-1-TIC, and the noise under the corresponding CTL value was recorded at the same time. The results are shown in Figure 4b. From Figure 4b, the CTL intensity of toluene increased with an increase in the gas flow rate below 300 mL/min, and the S/N first increased with the increase in gas flow rate and then decreased after 200 mL/min. Therefore, the gas flow rate of 200 mL/min was chosen for detection because of the resulting strong and steady CTL signals.

3.4. Analytical Characteristics

Under the optimal experimental conditions, the analytical characteristics of the CTL sensor based on Pt/Ti₃C₂T_x-CNT toward toluene were studied. A response curve obtained from the different concentrations of toluene is shown in Figure 5, indicating a good linear relationship within the concentration range of 2.5~87 ppm. The limit of detection defined as 3 S/N was about 2 ppm. The linear regression equation was $y = 2034x - 4858.3$ ($2.5 \leq x \leq 87$ ppm, $R^2 = 0.9228$), where y represents the average relative intensity of CTL after three parallel experiments, and x represents the concentration of toluene.

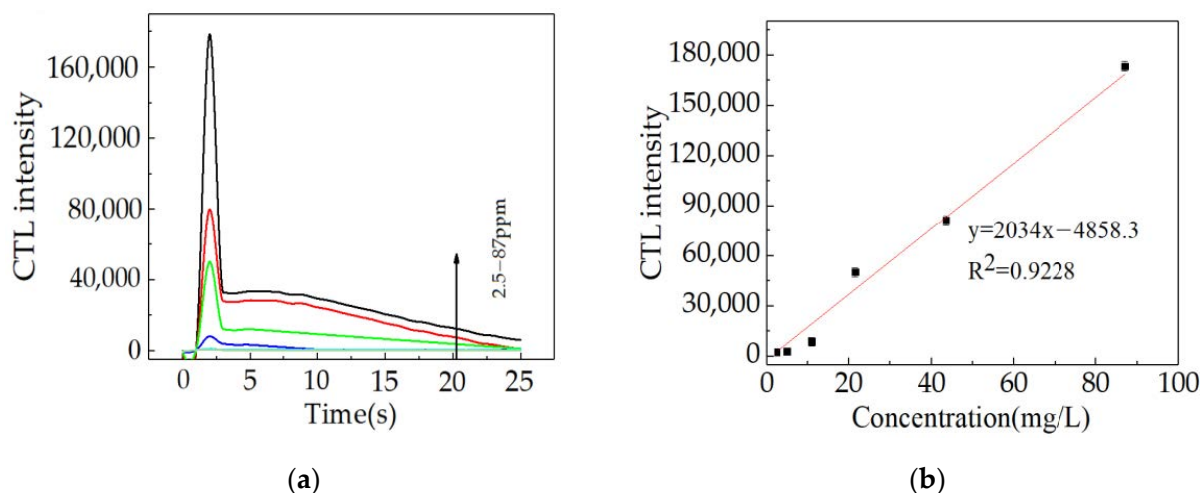


Figure 5. (a) Effects of analyte concentration on CTL intensity; (b) correlation curve of response signal intensity of different concentrations of toluene on the surface of Pt/Ti₃C₂T_x-CNT materials. (working temperature: 150 °C; airflow rate: 200 mL/min).

3.5. Selectivity and Stability of the Pt/Ti₃C₂T_x-CNT for Toluene

In addition to good reproducibility, excellent selectivity is also critical for the sensor, especially for practical detection. Under suitable conditions, 10 VOCs (toluene, trichloromethane, tetrachloroethane, cyclohexane, formaldehyde, diethyl ether, acetone, carbon dioxide, ammonia, and ethanol) were introduced into the reaction chamber to prove the selectivity of Pt/Ti₃C₂T_x-CNT. The CTL intensity of seven VOCs on the surface of the material is shown in Figure 6a. From Figure 6a, except for toluene and formaldehyde, the other eight VOCs had no obvious response on the Pt/Ti₃C₂T_x-CNT surface. There was no evident interference in the detection of toluene. Therefore, Pt/Ti₃C₂T_x-CNT has good selectivity in the detection of toluene.

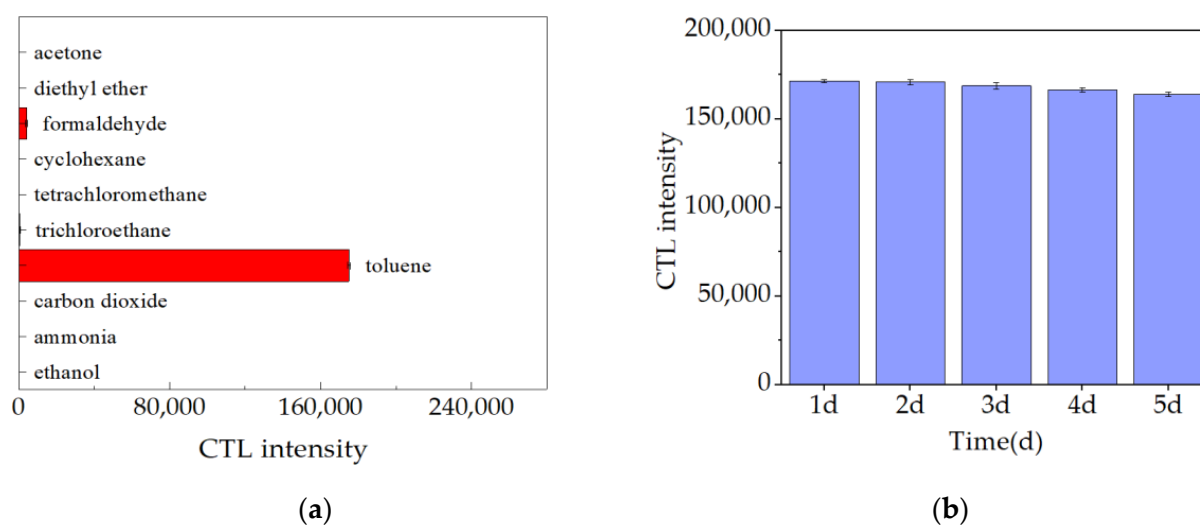


Figure 6. (a) Selectivity of the Pt/Ti₃C₂T_x-CNT for toluene; (b) stability of the Pt/Ti₃C₂T_x-CNT for toluene (detecting concentration: 87 ppm; working temperature: 150 °C; airflow rate: 200 mL/min).

In order to verify the stability of the continuous operation of Pt/Ti₃C₂T_x-CNT at the optimal temperature (150 °C), the sensing performance of Pt/Ti₃C₂T_x-CNT to toluene was measured working for 8 h every day. The average value of the measurement was taken as the measurement result of the day, working continuously for 5 days, and the error is shown by the error bar. As shown in Figure 6b, the results revealed that the CTL intensity produced by toluene on the surface of the material was 171,500 on the first day, and it slightly decreased over the next few days. After 5 days, the CTL intensity produced by toluene on the surface of the material was 164,000, and the signal intensity of toluene decreased by 4.37% after 5 consecutive days. In addition, the XRD pattern of Pt/Ti₃C₂T_x-CNT after its continuous operation is shown in Figure 2b. There was no obvious difference between the fresh Pt/Ti₃C₂T_x-CNT and the one after detection. This indicates that the CTL sensor has high stability.

3.6. The Advantages of Pt/Ti₃C₂T_x-CNT Sensor

Table 2 shows the analytical characteristics of the sensor presented here and some previously reported sensors. As shown in Table 2, the Pt/Ti₃C₂T_x-CNT sensor has a faster response, shorter recovery time, and lower working temperature compared with previous reports. The fast response and recovery time of this sensor greatly improve its detection efficiency, and its lower working temperature can reduce the energy consumption of the detection process. Therefore, Pt/Ti₃C₂T_x-CNT has great advantages in detecting toluene. In addition, Pt/Ti₃C₂T_x-CNT contains the advantages from each component, enabling a possible coordination effect to achieve high catalytical performance. CNT provides a large sensing area for the CTL reaction. Ti₃C₂T_x makes the material junction more stable.

Moreover, the Pt attached to the surface can provide excited electrons according to the principle of catalytic luminescence detection [19].

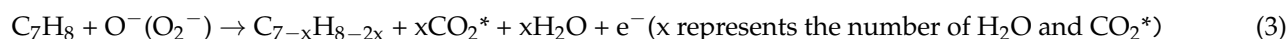
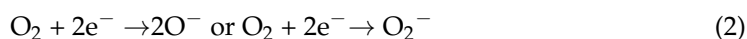
Table 2. Reports on the detection of toluene based on CTL in recent years.

Principle	Sensing Material	Response Time (s)	Recovery Time (s)	Temperature (°C)	Reference
CTL	TiO ₂ /SnO ₂	ND	ND	270	[42]
CTL	γ-Al ₂ O ₃ /PtO ₂	1.5	60	236	[43]
CTL	Al ₂ O ₃ /Pt	2	38	395	[19]
CTL	γ-Al ₂ O ₃ /Eu ₂ O ₃	3	30	432	[16]
CTL	Pt/Ti ₃ C ₂ T _x -CNT	1	30	150	This work

3.7. Possible Mechanism

Different metal-based catalysts have been found for the detection of VOCs, and their presence in nanomaterials can enhance the sensing characteristics of sensors. Firstly, due to the adsorption of methyl, the adsorption of toluene on the sensor surface is enhanced. Secondly, in our study, considering the interaction between -CH₃ and Pt, electrons more easily transition from the π_{CH₃} level to the Fermi level and from the Fermi level to the π_{CH₃*} level. Therefore, the adsorption barrier of toluene becomes lower, and the electronic effect between methyl and Pt is enhanced [46,47]. From the perspective of the through-space effect, there is through-space repulsion between -CH₃ and Pt, which is not conducive to the adsorption of -CH₃ and Pt [48]. Therefore, this indicates that Ti₃C₂T_x and CNT accelerate the conduction of electrons, change the working function and adsorption barriers, and make the electronic effect more dominant than the spatial effect, thus improving the sensor response. Moreover, the CNT-binding Ti₃C₂T_x provides greater contact space for gas molecules [26,30].

It is worth noting that only the materials located at the surface of the sensing layer can make contact with the gas analytes effectively. Hence, it is assumed that the produced CTL signal is the result of the reaction of toluene and oxygen in the surface layer of the material. The whole process of CTL response is described as follows:



Firstly, toluene and oxygen in the air are adsorbed on the surface of Pt/Ti₃C₂T_x-CNT. Oxygen adsorbed on the surface of catalyst at appropriate temperature receives free electrons to form oxygen ions (O⁻ and O₂⁻) [39,49,50]. Secondly, toluene adsorbed on the surface of Pt/Ti₃C₂T_x-CNT is catalytically oxidized with O⁻ and O₂⁻, and the reaction products then diffuse into the gas phase. In the process of catalytic oxidation reaction, excited CO₂ (CO₂^{*}) is generated, and the returning process of the released CO₂^{*} photons to the ground state (CO₂) is accompanied by the generation of optical signals. The main mechanism of CTL signal generation is that the catalyst catalyzes the generation of excited states and converts energy into optical signals [51–54].

4. Conclusions

In this study, a sensor based on Pt/Ti₃C₂T_x-CNT was developed for the detection of toluene without the aid of biological reagent identification or instrumental separation. Pt/Ti₃C₂T_x-CNT exhibited the best catalytic performance toward toluene due to its large specific surface area and stable structure. The gas sensor based on Pt/Ti₃C₂T_x-CNT has the advantage of rapid response. Additionally, the material has a wide scope of detection for toluene, and the optimal working temperature (150 °C) is lower compared with common sensors, so it has a broad prospect in the actual detection process. The limit of detection defined as 3 S/N was about 2 ppm. The possible sensing mechanism of CTL showed that

toluene was oxidized to generate excited-state CO_2^* , which emitted a luminescent signal when it returned to the ground state.

Author Contributions: Conceptualization, H.W. and B.S.; validation, B.S.; formal analysis, X.S. and F.L.; writing—original draft preparation, H.W. and B.S.; writing—review and editing, B.S.; supervision, B.S.; project administration, T.D.; funding acquisition, B.S. All authors have read and agreed to the published version of the manuscript.

Funding: This work was supported by the Project of the National Key Research and Development Program (2019YFC0408505), the Natural Science Research Project of the Higher Education Institutions of Anhui Province (KJ2021A0303, KJ2021A0616), the Science and Technology Major projects of Anhui Province (18030801106), the teaching research project of Anhui Province (2019jyxm0994), the first batch of natural science projects supported by surplus funds in 2021 of Anhui Jianzhu University (JZ202129, JZ202134), and the Scientific Research Start-up Foundation for Introduction of Talent, Anhui Jianzhu University (2016QD113).

Institutional Review Board Statement: Not applicable.

Informed Consent Statement: Not applicable.

Data Availability Statement: Not applicable.

Conflicts of Interest: The authors declare no conflict of interest.

References

1. Kim, K.H.; Jahan, S.A.; Kabir, E. A review of breath analysis for diagnosis of human health. *TrAC Trends Anal. Chem.* **2012**, *33*, 1–8. [[CrossRef](#)]
2. Amann, A.; Corradi, M.; Mazzone, P.; Mutti, A. Lung cancer biomarkers in exhaled breath. *Expert Rev. Mol. Diagn.* **2011**, *11*, 207–217. [[CrossRef](#)] [[PubMed](#)]
3. Konvalina, G.; Haick, H. Sensors for breath testing: From nanomaterials to comprehensive disease detection. *Acc. Chem. Res.* **2014**, *47*, 66–76. [[CrossRef](#)] [[PubMed](#)]
4. Zhang, Z.; Zhu, L.; Wen, Z.; Ye, Z. Controllable synthesis of Co_3O_4 crossed nanosheet arrays toward an acetone gas sensor. *Sens. Actuators B Chem.* **2017**, *238*, 1052–1059. [[CrossRef](#)]
5. Qin, W.; Yuan, Z.; Shen, Y.; Zhang, R.; Meng, F. Phosphorus-doped porous perovskite $\text{LaFe}_{1-x}\text{P}_x\text{O}_{3-\delta}$ nanosheets with rich surface oxygen vacancies for ppb level acetone sensing at low temperature. *Chem. Eng. J.* **2022**, *431*, 134280. [[CrossRef](#)]
6. Xiong, Y.; Zhu, Z.; Ding, D.; Lu, W.; Xue, Q. Multi-shelled ZnCo_2O_4 yolk-shell spheres for high-performance acetone gas sensor. *Appl. Surf. Sci.* **2018**, *443*, 114–121. [[CrossRef](#)]
7. David, S.S.; Veeralakshmi, S.; Sandhya, J.; Nehru, S.; Kalaiselvam, S. Room temperature operable high sensitive toluene gas sensor using chemiresistive $\text{Ag}/\text{Bi}_2\text{O}_3$ nanocomposite. *Sens. Actuators B Chem.* **2020**, *320*, 128410. [[CrossRef](#)]
8. Healy, R.M.; Wang, J.M.; Karellas, N.S.; Todd, A.; Sofowote, U.; Su, Y.; Munoz, A. Assessment of a passive sampling method and two on-line gas chromatographs for the measurement of benzene, toluene, ethylbenzene and xylenes in ambient air at a highway site. *Atmos. Pollut. Res.* **2019**, *10*, 1123–1127. [[CrossRef](#)]
9. Douberly, G.E.; Ricks, A.M.; Schleyer PV, R.; Duncan, M.A. Infrared spectroscopy of gas phase benzenium ions: Protonated benzene and protonated toluene, from 750 to 3400 cm^{-1} . *J. Phys. Chem. A* **2008**, *112*, 4869–4874. [[CrossRef](#)]
10. Ji, J.; Deng, C.; Shen, W.; Zhang, X. Field analysis of benzene, toluene, ethylbenzene and xylene in water by portable gas chromatography-microflame ionization detector combined with headspace solid-phase microextraction. *Talanta* **2006**, *69*, 894–899. [[CrossRef](#)]
11. Lin, H.; Jang, M.; Suslick, K.S. Preoxidation for colorimetric sensor array detection of VOCs. *J. Am. Chem. Soc.* **2011**, *133*, 16786. [[CrossRef](#)] [[PubMed](#)]
12. Iwaki, T.; Covington, J.A.; Udrea, F.; Gardner, J.W. Identification and quantification of different vapours using a single polymer chemoresistor and the novel dual transient temperature modulation technique. *Sens. Actuators B Chem.* **2009**, *141*, 370–380. [[CrossRef](#)]
13. Breyse, M.; Claudel, B.; Faure, L.; Guenin, M.; Williams, R.J.; Wolkenstein, T. Chemiluminescence during the catalysis of carbon monoxide oxidation on a thoria surface. *J. Catal.* **1976**, *45*, 137–144. [[CrossRef](#)]
14. Zhou, K.; Xu, J.; Gu, C.; Liu, B.; Peng, Z. Identification and determination of formaldehyde, benzene and ammonia in air based on cross sensitivity of cataluminescence on single catalyst. *Sens. Actuators B Chem.* **2017**, *246*, 703–709. [[CrossRef](#)]
15. Almasian, M.R.; Na, N.; Wen, F.; Zhang, S.; Zhang, X. Development of a plasma-assisted cataluminescence system for benzene, toluene, ethylbenzene, and xylenes analysis. *Anal. Chem.* **2010**, *82*, 3457. [[CrossRef](#)] [[PubMed](#)]
16. Lu, J.; Cao, X.; Pan, C.; Yang, L.; Lai, G.; Chen, J.; Wu, C. Studies of the Cataluminescence of Benzene Homologues on Nanosized $\gamma\text{-Al}_2\text{O}_3/\text{Eu}_2\text{O}_3$ and the Development of a Gas Sensor for Benzene Homologue Vapors. *Sensors* **2006**, *6*, 1827–1836. [[CrossRef](#)]

17. Zeng, B.; Zhang, L.; Wan, X.; Song, H.; Lv, Y. Fabrication of α -Fe₂O₃/g-C₃N₄ composites for cataluminescence sensing of H₂S. *Sens. Actuators B Chem.* **2015**, *211*, 370–376. [[CrossRef](#)]
18. Leghrib, R.; Felten, A.; Demoisson, F.; Reniers, F.; Pireaux, J.J.; Llobet, E. Room-temperature, selective detection of benzene at trace levels using plasma-treated metal-decorated multiwalled carbon nanotubes. *Carbon* **2010**, *48*, 3477–3484. [[CrossRef](#)]
19. Wang, N.J.; Cao, X.A.; He, R.W.; Liu, Y.H.; Huang, Y.J. A cataluminescence-based sensor for detecting benzene, toluene and xylene vapors utilizing the catalytic reduction on the surface of nanosized Al₂O₃/Pt. *Adv. Mat. Res.* **2013**, *663*, 335–342.
20. Shi, Z.; Li, G.; Hu, Y. Cataluminescence sensor based on Pt/NU-901 nanocomposite for rapid capture, catalysis and detection of acetone in exhaled breath. *Anal. Chim. Acta* **2022**, *1206*, 339787. [[CrossRef](#)]
21. Zhang, R.K.; Wang, D.; Wu, Y.J.; Hu, Y.H.; Chen, J.Y.; He, J.C.; Wang, J.X. A Cataluminescence Sensor Based on NiO Nanoparticles for Sensitive Detection of Acetaldehyde. *Molecules* **2020**, *25*, 1097. [[CrossRef](#)] [[PubMed](#)]
22. Shi, G.; Sun, B.; Jin, Z.; Liu, J.; Li, M. Synthesis of SiO₂/Fe₃O₄ nanomaterial and its application as cataluminescence gas sensor material for ether. *Sens. Actuators B Chem.* **2012**, *171–172*, 699–704. [[CrossRef](#)]
23. Rushi, A.D.; Datta, K.P.; Ghosh, P.; Mulchandani, A.; Shirsat, M.D. Exercising substituents in porphyrins for real time selective sensing of volatile organic compounds. *Sens. Actuators B Chem.* **2018**, *257*, 389–397. [[CrossRef](#)]
24. Bao, Y.; Xu, P.; Cai, S.; Yu, H.; Li, X. Detection of volatile-organic-compounds (VOCs) in solution using cantilever-based gas sensors. *Talanta* **2018**, *182*, 148–155. [[CrossRef](#)] [[PubMed](#)]
25. Zhang, R.; Li, G.; Hu, Y. Simple and excellent selective chemiluminescence based CS₂ on line detection system for rapid analysis of sulfur-containing compounds in complex samples. *Anal. Chem.* **2015**, *87*, 5649–5655. [[CrossRef](#)]
26. Xu, M.; Liang, L.; Qi, J.; Wu, T.; Zhou, D.; Xiao, Z. Intralayered Ostwald Ripening-Induced Self-Catalyzed Growth of CNTs on MXene for Robust Lithium–Sulfur Batteries. *Small* **2021**, *17*, 2007446. [[CrossRef](#)]
27. Lin, H.; Wang, X.; Yu, L.; Chen, Y.; Shi, J. Two-Dimensional Ultrathin MXene Ceramic Nanosheets for Photothermal Conversion. *Nano Lett.* **2017**, *17*, 384–391. [[CrossRef](#)]
28. Anasori, B.; Lukatskaya, M.R.; Gogotsi, Y. 2D metal carbides and nitrides (MXenes) for energy storage. *Nat. Rev. Mater.* **2017**, *2*, 16098. [[CrossRef](#)]
29. Tao, Q.; Dahlqvist, M.; Lu, J.; Kota, S.; Meshkian, R.; Halim, J.; Palisaitis, J.; Hultman, L.; Barsoum, M.W.; Persson, P.O.; et al. Two-dimensional Mo_{1.33}C MXene with divacancy ordering prepared from parent 3D laminate with in-plane chemical ordering. *Nat. Commun.* **2017**, *8*, 14949. [[CrossRef](#)]
30. Zhou, J.; Zha, X.; Zhou, X.; Chen, F.; Gao, G.; Wang, S.; Shen, C.; Chen, T.; Zhi, C.; Eklund, P.; et al. Synthesis and Electrochemical Properties of Two-Dimensional Hafnium Carbide. *ACS Nano* **2017**, *11*, 3841–3850. [[CrossRef](#)]
31. Zhou, Y.; Jiang, Y.; Xie, G.; Du, X.; Tai, H. Gas sensors based on multiple-walled carbon nanotubes-polyethylene oxide films for toluene vapor detection. *Sens. Actuators B Chem.* **2014**, *191*, 24–30. [[CrossRef](#)]
32. Crescitelli, A.; Consales, M.; Penza, M.; Aversa, P.; Giordano, M.; Cusano, A. Toluene detection in aqueous phase by optical fiber sensors integrated with single-walled carbon nanotubes. *Open Environ. Biol. J.* **2008**, *1*, 26–32.
33. Firouzjaei, M.D.; Karimiziarani, M.; Moradkhani, H.; Elliott, M.; Anasori, B. MXenes: The two-dimensional influencers. *Mater. Today Adv.* **2022**, *13*, 100202. [[CrossRef](#)]
34. Yu, L.; Li, N. Noble Metal Nanoparticles-Based Colorimetric Biosensor for Visual Quantification: A Mini Review. *Chemosensors* **2019**, *7*, 53. [[CrossRef](#)]
35. Kim, H.W.; Lee, J.W. GeO₂ nanostructures fabricated by heating of Ge powders: Pt-catalyzed growth, structure, and photoluminescence. *Phys. E Low-Dimens. Syst. Nanostruct.* **2008**, *40*, 2499–2503. [[CrossRef](#)]
36. Shi, Z.; Xia, L.; Li, G.; Hu, Y. Pt/Au Nanoparticles@Co₃O₄ Cataluminescence Sensor for Rapid Analysis of Methyl Sec-Butyl Ether Impurity in Methyl Tert-Butyl Ether Gasoline Additive. *Chemosensors* **2022**, *10*, 260. [[CrossRef](#)]
37. Alhabeib, M.; Maleski, K.; Mathis, T.S.; Sarycheva, A.; Hatter, C.B.; Uzun, S.; Levitt, A.; Gogotsi, Y. Selective etching of silicon from Ti₃SiC₂ (MAX) to obtain 2D titanium carbide (MXene). *Angew. Chem. Int. Edit.* **2018**, *57*, 5444–5448. [[CrossRef](#)]
38. Xie, X.; Zhao, M.Q.; Anasori, B.; Maleski, K.; Ren, C.E.; Li, J.; Byles, B.W.; Pomerantseva, E.; Wang, G.; Gogotsi, Y. Porous heterostructured MXene/carbon nanotube composite paper with high volumetric capacity for sodium-based energy storage devices. *Nano Energy* **2016**, *26*, 513–523. [[CrossRef](#)]
39. Xu, C.; Fan, C.; Zhang, X.; Chen, H.; Liu, X.; Fu, Z.; Wang, R.; Hong, T.; Cheng, J. MXene (Ti₃C₂T_x) and carbon nanotube hybrid-supported platinum catalysts for the high-performance oxygen reduction reaction in PEMFC. *ACS Appl. Mater. Interfaces* **2020**, *12*, 19539–19546. [[CrossRef](#)]
40. Meng, F.; Qi, T.; Zhang, J.; Zhu, H.; Yuan, Z.; Liu, C.; Qin, W.; Ding, M. MoS₂-Templated Porous Hollow MoO₃ Microspheres for Highly Selective Ammonia Sensing via a Lewis Acid-Base Interaction. *IEEE Trans. Ind. Electron.* **2022**, *69*, 960–970. [[CrossRef](#)]
41. Wu, M.; Park, H.; Cho, K.M.; Kim, J.Y.; Kim, S.J.; Choi, S.; Kang, Y.; Kim, J.; Jung, H.T. Formation of toroidal Li₂O₂ in non-aqueous Li–O₂ batteries with Mo₂CT_x MXene/CNT composite. *RSC Adv.* **2019**, *9*, 41120–41125. [[CrossRef](#)]
42. Sha, W.; Ni, S.; Zheng, C. Development of cataluminescence sensor system for benzene and toluene determination. *Sens. Actuators B Chem.* **2015**, *209*, 297–305. [[CrossRef](#)]
43. Sun, Y.; Cao, X.; Liu, Y.; Wang, N.; He, R. Research on benzene, toluene and dimethylbenzene detection based on a cataluminescence sensor. *Luminescence* **2014**, *29*, 122–126. [[CrossRef](#)]
44. Sharma, C.S.; Katapalli, H.; Sharma, A.; Madou, M. Fabrication and electrical conductivity of suspended carbon nanofiber arrays. *Carbon* **2011**, *49*, 1727–1732. [[CrossRef](#)]

45. Huang, X.; Song, H.; Zhang, L.; Deng, D.; Lv, Y. ZnO Nanoparticle-Decorated CeO₂ Nanospheres for Cataluminescence Sensing of H₂S. *ACS Appl. Nano Mater.* **2021**, *4*, 9557–9565. [[CrossRef](#)]
46. Minot, C.; Gallezot, P. Competitive hydrogenation of benzene and toluene: Theoretical study of their adsorption on ruthenium, rhodium, and palladium. *J. Catal.* **1990**, *123*, 341–348. [[CrossRef](#)]
47. Kwon, Y.J.; Na, H.G.; Kang, S.Y.; Choi, S.W.; Kim, S.S.; Kim, H.W. Selective detection of low concentration toluene gas using Pt-decorated carbon nanotubes sensors. *Sens. Actuators B Chem.* **2016**, *227*, 157–168. [[CrossRef](#)]
48. Orozco, J.M.; Webb, G. The adsorption and hydrogenation of benzene and toluene on alumina- and silica- supported palladium and platinum catalysts. *Appl. Catal.* **1983**, *6*, 67–84. [[CrossRef](#)]
49. Qin, W.; Yuan, Z.; Gao, H.; Zhang, R.; Meng, F. Perovskite-structured LaCoO₃ modified ZnO gas sensor and investigation on its gas sensing mechanism by first principle. *Sens. Actuators B Chem.* **2021**, *341*, 130015. [[CrossRef](#)]
50. Meng, F.; Li, X.; Yuan, Z.; Lei, Y.; Qi, T.; Li, J. Ppb-Level Xylene Gas Sensors based on Co₃O₄ Nanoparticles coated Reduced Graphene Oxide (rGO) Nanosheets Operating at Low Temperature. *IEEE Trans. Instrum. Meas.* **2021**, *70*, 9511510. [[CrossRef](#)]
51. Yu, K.; Hu, J.; Li, X.; Zhang, L.; Lv, Y. Camellia-like NiO: A novel cataluminescence sensing material for H₂S. *Sens. Actuators B Chem.* **2019**, *288*, 243–250. [[CrossRef](#)]
52. Cao, X.; Zhang, Z.; Zhang, X. A novel gaseous acetaldehyde sensor utilizing cataluminescence on nanosized BaCO₃. *Sens. Actuators B Chem.* **2004**, *99*, 30–35. [[CrossRef](#)]
53. Ye, Q.; Gao, Q.; Zhang, X.R.; Xu, B.Q. Cataluminescence and catalytic reactions of ethanol oxidation over nanosized Ce_{1-x}Zr_xO₂ (0 ≤ x ≤ 1) catalysts. *Catal. Commun.* **2006**, *7*, 589–592. [[CrossRef](#)]
54. Wang, S.; Yuan, Z.; Zhang, L.; Lin, Y.; Lu, C. Recent advances in cataluminescence-based optical sensing systems. *Analyst* **2017**, *142*, 1415–1428. [[CrossRef](#)]